Evolution of entropy in the outer heliosphere

Evolution of entropy in the outer heliosphere

L Adhikari[1], G P Zank[1,2], L -L Zhao[1], and G M Webb [1]

[1]Center for Space Plasma and Aeronomic Research (CSPAR), University of Alabama in Huntsville, Huntsville,
AL 35899, USA
[2]Department of Space Science, University of Alabama in Huntsville, Huntsville, AL 35899, USA

E-mail: la0004@uah.edu

Abstract. Entropy is an important thermodynamic quantity. Based on the conservation equations of a coupled solar wind and turbulence model, and using measurements from Voyager 2, Pioneer 10 and New Horizons, we investigate the solar wind entropy throughout the heliosphere. Observations from Voyager 2, Pioneer 10, and the NH SWAP instrument show different radial profiles of the entropy as a function of heliocentric distance. We find that the entropy measured by (i) Voyager 2 increases by about 12.84% at 75 au, (ii) NH SWAP increases by about 7.8% at 46.37 au, and (iii) Pioneer 10 increases by about 6.5% at 56.82 au. Voyager 2 and NH SWAP made measurements in the upwind direction and Pioneer 10 is in the downwind direction. We compare directly the theoretical results with Voyager 2 measurements only, and find good agreement between them.

1. Introduction

Entropy is an important thermodynamic quantity. If the system follows the ideal gas law, the entropy of the system is defined by $S = c_v \log(P/\rho^\gamma)$, where $P(= 2nk_BT)$ is the thermal pressure (scalar), T is the proton (isotropic) temperature, n is the solar wind proton density, ρ is the solar wind mass density, k_B is the Boltzmann constant, γ is a polytropic constant, and c_v is a specific heat constant. Here the ideal gas law means that the distribution function satisfies the Maxwellian distribution. However, if the distribution function follows a kappa distribution, the entropy S_κ is defined by $S = \log[1 - (1/\kappa)S_\kappa/k_B]^{-\kappa}$, where κ is the kappa index [1]. In this manuscript, we use the Maxwellian distribution definition to calculate the theoretical and observed solar wind entropy. The thermal pressure and solar wind mass density are directly obtained from the theoretical solutions and spacecraft measurements. For the polytropic index, we use $\gamma = 5/3$. The polytropic index can have different values, ranging from 0.5 to 2.5, with a mean value of 1.66 [1–3].

Recently, Adhikari et al [5] studied the evolution of the solar wind entropy in the outer heliosphere using conservative solar wind and turbulence transport model equations and compared their solutions to Voyager 2 (V2) measurements. They found that the solar wind entropy increases by about 12.84% at 75 au. The increase in entropy is due to the dissipation of turbulence. Whang et al [6,7] considered the entropy increase across a shock in the solar wind, finding an increase of about 0.8×10^{-23} J/K/proton due to shock wave heating. By simulating shock propagation throughout the solar wind, based on Helios A, Helios B, Voyager 2, Voyager 1, Pioneer 10 and Pioneer 11 measurements, Whang et al argued that if the heliocentric distance is increased by about 10 times, the entropy increases by about 4×10^{-23} J/K/proton.

In this paper, we study the evolution of entropy in the solar wind observationally in the upwind and downwind directions using Voyager 2 (V2) and New Horizons Solar Wind Around Pluto (NH SWAP) measurements, and Pioneer 10 (P10) measurement, respectively. The theoretical evolution of entropy is modeled using the conservative solar wind and turbulence transport model equations of Adhikari et al [5]. The turbulence transport model equations are based on the Zank et al [8] turbulence transport model theory. Adhikari et al showed that the sum of the solar wind energy and the turbulent energy is constant.

We organize the manuscript as follows. In Section 2, we present the model equations, and discuss both modeled and observed results in Section 3. Finally, we present the discussion and conclusions in Section 4.

2. Theoretical Model Equations

Theoretical and observational studies show that the solar wind speed in the outer heliosphere is reduced by about 15% due to the pick up of interstellar neutral gas [9–11]. The kinetic energy of the solar wind accordingly decreases in the outer heliosphere. Other large scale physical processes, such as the interactions of streams may absorb some of the energy of the bulk solar wind flow converting it to heating and turbulence, resulting a decrease in the solar wind speed. A 1D steady-state momentum equation that including the loss of momentum due to the pick up of interstellar neutral gas and the interaction of streams is given by [5]

$$\rho U \frac{dU}{dr} = -\frac{dP}{dr} - \frac{\rho}{U} S^{shear} - \frac{\rho}{U} S^{PUI}. \tag{1}$$

The second and third terms on the rhs of Equation (1) are introduced by dimensional analysis. The second term is associated with the driving of turbulent fluctuations by, e.g., a Kelvin-Helmholtz instability driven by stream-shear and the third term is associated with the instability generated by new born pickup ions in the outer heliosphere. We do not include the magnetic field in Equation (1), and consider a simple hydrodynamic model. Equation (1) can be written as [5],

$$\frac{1}{r^2}\frac{d}{dr}\left(r^2 \rho U \frac{U^2}{2}\right) = -U\frac{dP}{dr} - \rho S^{shear} - \rho S^{PUI}, \tag{2}$$

where $r^2\rho U$ is a (constant) mass flux. The evolution of the solar wind thermal pressure can be expressed as [5]

$$\frac{1}{r^2}\frac{d}{dr}\left(\rho U r^2 \frac{\gamma}{\gamma-1}\frac{P}{\rho}\right) = U\frac{dP}{dr} + S_t, \tag{3}$$

where S_t is a turbulent heating term. Since the rhs terms of Equations (2) and (3) show that the solar wind equations are affected by turbulence, we introduce the turbulence transport model equations. Based on the turbulence transport model equations of Zank et al [8] (see also [12]), Adhikari et al [5] derived two coupled turbulence transport equations for the fluctuating magnetic energy density and the correlation length for two cases (i) when the turbulence is dominated by the fluctuating magnetic energy [9,13–15], which is related to quasi-2D magnetic turbulence [13], and (ii) when the fluctuating kinetic and magnetic energies are equipartitioned due to the excitation of Alfvén waves by the pickup process, which is similar to nearly incompressible NI/slab magnetic turbulence [13]. Here, case (i) is more appropriate within $\sim 5-7$ au where the stream-shear source of turbulence is dominant, and case (ii) is more appropriate in the outer heliosphere in the upwind direction where the pickup ion source of turbulence is important.

For case (i), the two coupled 1D steady-state turbulence transport equations for the fluctuating magnetic energy density E_b^0 and the correlation length λ_b^0 are given by [5,12],

$$\frac{1}{r^2}\frac{d}{dr}\left(r^2\rho U E_b^0\right) = -\rho\frac{{E_b^0}^{3/2}}{\lambda_b^0} + \rho C_{sh}\frac{\Delta U V_{A0}^2 r_0}{r^2}; \tag{4}$$

$$U\frac{d\lambda_b^0}{dr} = \frac{E_b^0}{2} - \frac{\lambda_b^0}{2E_b^0}C_{sh}\frac{\Delta U V_{A0}^2 r_0}{r^2}, \tag{5}$$

where the first term on the rhs of Equation (4) describes the dissipation of turbulence based on a Kolmogorov phenomenology [8,12,19]. The parameter C_{sh} defines the strength of the stream-shear source of turbulence, ΔU is the difference between the fast and slow solar wind speed, and V_{A0} is the Alfvén velocity at a reference point r_0.

For case (ii), the two coupled turbulence transport model equations for the fluctuating NI/slab magnetic energy density and the correlation length are given by [5,12]

$$\begin{aligned}\frac{1}{r^2}\frac{d}{dr}\left[r^2\rho U E_b^{A0}\log\left(\frac{\bar{E}_b^A}{\bar{\rho}^{1/2}}\right)\right] &= -\rho\frac{\sqrt{2}E_b^{A0}{E_b^A}^{1/2}}{\lambda_b^A} \\ &\quad + \frac{\rho E_b^{A0}}{2E_b^A}\frac{f_D n_H^\infty U V_{A0}}{n_{sw}^0\tau_{ion}^0}\exp\left(-\frac{L}{r}\right);\end{aligned} \tag{6}$$

$$U\frac{d\lambda_b^A}{dr} = \frac{{E_b^A}^{1/2}}{\sqrt{2}} - \frac{\lambda_b^A}{4E_b^A}\frac{f_D n_H^\infty U V_{A0}}{n_{sw}^0\tau_{ion}^0}\exp\left(-\frac{L}{r}\right). \tag{7}$$

See [5] for the derivation of the Equations (4–7). Here, $\bar{E}_b^A = E_b^A/E_b^{A0}$ and $\bar{\rho} = \rho/\rho_0$, where E_b^{A0} and ρ_0 are the NI/slab fluctuating magnetic energy density and the solar wind density at 1 au. The parameter f_D represents the fraction of the pickup ion source

of turbulence that drives turbulence in the outer heliosphere [16], n_H^{∞} is the neutral hydrogen density, τ_{ion}^0 is the neutral H ionization time at 1 au, n_{sw}^0 is the solar wind density at 1 au, and L is the ionization cavity length scale. Adding Equations (2), (3), (4), and (6), we obtain

$$\begin{aligned}\frac{1}{r^2}\frac{d}{dr}\left[r^2\rho U\left(\frac{U^2}{2}+\frac{\gamma}{\gamma-1}\frac{P}{\rho}+E_b^0+E_b^{A0}\log\left(\frac{\bar{E}_b^A}{\bar{\rho}^{1/2}}\right)\right)\right]\\ =\left(S_t-\rho\frac{E_b^{3/2}}{\lambda_b^0}-\rho\frac{\sqrt{2}E_b^{A0}E_b^{A\,1/2}}{\lambda_b^A}\right)\\ -\rho\left(S^{shear}-C_{sh}\frac{\Delta UV_{A0}^2r_0}{r^2}\right)\\ -\rho\left(S^{PUI}-\frac{E_b^{A0}}{2E_b^A}\frac{f_Dn_H^{\infty}UV_{A0}}{n_{sw}^0\tau_{ion}^0}\exp\left(-\frac{L}{r}\right)\right),\end{aligned} \tag{8}$$

where, the terms in [...] denote the sum of the solar wind kinetic (flux) energy, enthalpy, and the magnetic turbulence energy (quasi-2D + NI/slab). Setting

$$S_t=\rho\frac{E_b^{3/2}}{\lambda_b^0}+\rho\frac{\sqrt{2}E_b^{A0}E_b^{A\,1/2}}{\lambda_b^A}; \tag{9a}$$

$$S^{shear}=C_{sh}\frac{\Delta UV_{A0}^2r_0}{r^2}; \tag{9b}$$

$$S^{PUI}=\frac{E_b^{A0}}{2E_b^A}\frac{f_Dn_H^{\infty}UV_{A0}}{n_{sw}^0\tau_{ion}^0}\exp\left(-\frac{L}{r}\right), \tag{9c}$$

where, Equation (9a) denotes the turbulent heating term [9,17], Equations (9b) and (9c) are the turbulence sources associated with the shear flow [13,15], and the pickup ions [9,12,14,15], respectively, we obtain the total energy conservation equation

$$\begin{aligned}&\frac{1}{r^2}\frac{d}{dr}\left[r^2\rho U\left(\frac{U^2}{2}+\frac{\gamma}{\gamma-1}\frac{P}{\rho}+E_b^0+E_b^{A0}\log\left(\frac{\bar{E}_b^A}{\bar{\rho}^{1/2}}\right)\right)\right]=0;\\ &\Rightarrow\frac{U^2}{2}+\frac{\gamma}{\gamma-1}\frac{P}{\rho}+E_b^0+E_b^{A0}\log\left(\frac{\bar{E}_b^A}{\bar{\rho}^{1/2}}\right)=const.\end{aligned} \tag{10}$$

Equation (10) shows that the sum of the kinetic energy (flux), enthalpy, and the (quasi-2D + NI/slab) fluctuating magnetic energy is constant. Equation (10) establishes that the decrease in the solar wind energy due to the instabilities associated with the shear flow and the isotropization of pickup ions drives magnetic turbulence in such a way that the total energy is always constant. The turbulent energy is then deposited back into the solar wind in the form of heat.

The evolution of the solar wind entropy is influenced by turbulence. The 1D steady-state solar wind entropy equation can be expressed as [5]

$$\frac{1}{r^2}\frac{d}{dr}(r^2\rho US)=(\gamma-1)c_v\frac{\rho}{P}S_t. \tag{11}$$

Equation (11) shows that the solar wind entropy is not constant, unlike in ideal MHD, where the entropy is constant [18]. Equation (11) shows that the entropy always increases for $\gamma > 1$, and decreases for $\gamma < 1$. We solve the coupled solar wind and turbulence transport model equations numerically by a Runge-Kutta 4th order method using the following boundary conditions at 1 au: $E_b^0 = 300$ km^{2}s^{-2}, $E_b^A = 6.12$ km^{2}s^{-2}, $\lambda_b^0 = 0.01$ au, $\lambda_b^A = 0.03$ au, $T = 9 \times 10^4$ K, $U = 420$ kms^{-1}, and $\rho = 7$ cm^{-3}. Similarly, we use $V_{A0} = 50$ kms^{-1}, $\Delta U = 200$ kms^{-1}, $n_H^\infty = 0.1$ cm^{-1}, $\tau_{ion} = 10^6$ s, $C_{sh} = 0.7$, $f_D = 0.4$, and $L = 7$ au.

3. Results

We present the numerical results, and compare the theoretical results with Voyager 2 (V2), Pioneer 10 (P10), and New Horizon Solar Wind Around Pluto (NH SWAP) measurements as a function of heliocentric distance. V2 and NH are traveling in the upwind direction and P10 in the downwind direction. Figure 1 displays the solar wind entropy as a function of heliocentric distance. The black curve denotes the theoretical solar wind entropy, showing that the entropy increases as $\sim r^{0.031}$, where r is heliocentric distance. The blue "*" denotes the entropy observed by V2, which shows that the radial profile of the observed entropy is similar to the black curve (theoretical entropy). Here the theoretical and observed solar wind entropy is calculated by $S \sim \log(P/\rho^\gamma)$. The red "*" indicates that the entropy measured by P10 increases in a similar fashion to that of the blue "*" until $\sim$ 32 au, after which the observed entropy slowly decreases until $\sim$ 40 au, and then flattens with increasing distance. It shows clearly that the entropy measured by P10 (red "*") deviates from the entropy measured by V2 (blue "*") beyond $\sim$ 32 au, and the entropy observed by prior measurement is lower than that measured by later measurement. Since the entropy is calculated by $S \sim \log(P/\rho^\gamma)$, therefore, any changes in P and ρ may also change the entropy. We discuss the observed solar wind parameters below. However, since the trajectory of P10 is in the downwind direction and remains within 10 degrees (latitude), while the trajectory of V2 is in the upwind direction and leaves the ecliptic plane after $\sim$ 35 au, solar wind turbulence may be different in the two directions, which may lead to different solar wind entropy in the upwind and downwind directions. A likely difference for the behavior of the entropy in the upwind and downwind directions is that the spatial distribution of neutral gas is different in the two directions.

The green "*" in Figure 1 denotes the entropy measured by NH SWAP as a function of heliocentric distance. Although the trajectories of V2 and NH SWAP are similar in the upwind direction, the entropy observed by NH SWAP is lower than that observed by V2, and the entropy increases monotonically and slowly with increasing distance. Similarly, the entropy observed by NH SWAP is relatively lower than that of P10 until $\sim$ 32 au, and then greater than P10. Adhikari et al [5] pointed out that the dissipation of turbulence increases the solar wind entropy for a polytropic index greater than $\gamma = 1$, but it is also affected by the solar wind density. The solar wind density observed by P10 and NH SWAP is higher than that observed by V2 (see Figure 2, top right), which results in lower values of the entropy along the trajectory of P10 and NH SWAP than V2.

Figure 2 compares the theoretical and observed solar wind plasma parameters. The

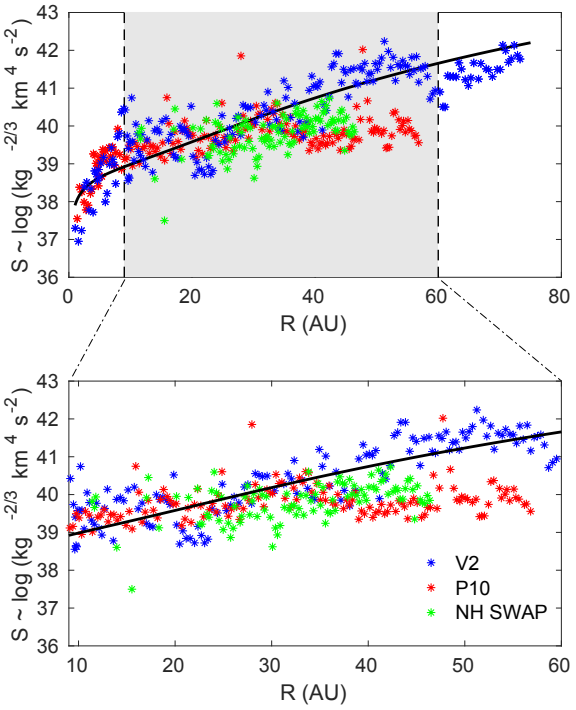

Figure 1. Comparison between the theoretical and observed solar wind entropy as a function of heliocentric distance. The solid curve denotes the theoretical entropy, the blue, red, and green "*" are the observed solar wind entropy corresponding to Voyager 2, Pioneer 10, and NH SWAP measurements, respectively.

black curve denotes the theoretical results, the blue "*" the V2 measurement, the red "*" the P10 measurement, and the green "*" the NH SWAP measurement. The top left panel of Figure 2 shows the solar wind speed as a function of heliocentric distance. The theoretical solar wind speed increases initially due to the pressure gradient, and then decreases very slowly with increasing heliocentric distance. The decrease in solar wind speed is due to the energy absorbed by the stream-shear and the pickup ion sources of turbulence. Note that the decreasing radial profile of the solar wind speed is not as obvious as in Zank et al [9], who developed a nearly incompressible MHD turbulence model to study the effect of pickup ions on the solar wind plasma, and found that the solar wind speed decreases by about 15% at 75 au [10,11]. Zank et al [9] included photoionization and charge exchange between the solar wind protons and interstellar neutrals in the momentum equation, resulting in a decrease in the solar wind speed. This model does not include these processes, but recognizes instead that the solar wind loses energy in driving turbulence, that then dissipates and heats the solar wind plasma. The solar wind speed measured by V2 shows that the speed varies between ~ 350 kms^{-1} and ~ 550 kms^{-1}. The observed solar wind speed by P10 is similar to that of V2 from 1

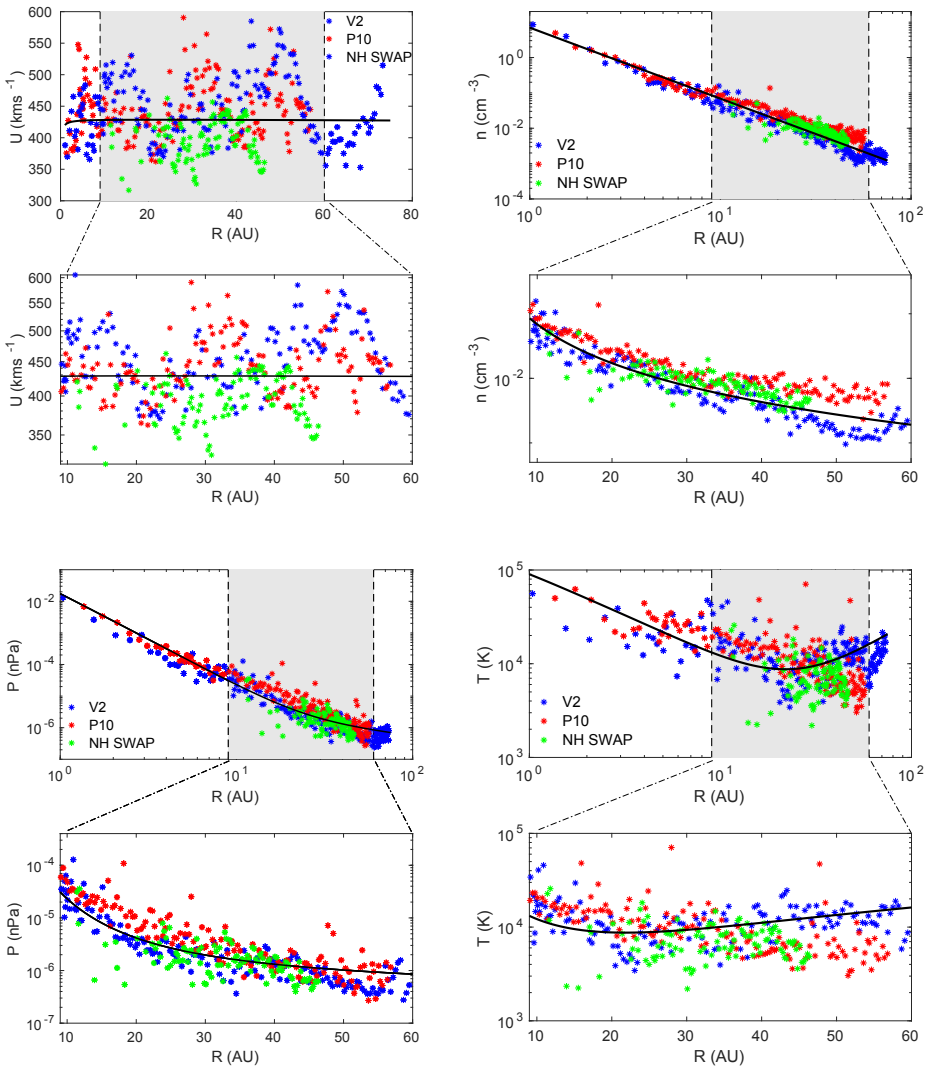

Figure 2. Top left: Solar wind speed as a function of heliocentric distance. Top right: Solar wind density as a function heliocentric. Bottom left: Solar wind pressure as a function of heliocentric distance. Bottom right: Solar wind temperature as a function of heliocentric distance. The convention for the figure is the same as used in Figure 1.

to ~ 10 au, and is smaller over the distance $\sim 10-18$ au. Similarly, the speed measured by P10 is similar to that observed by V2 until ~ 30 au, then higher until ~ 35 au, and then lower until ~ 55 au. NH SWAP mostly measures the slow solar wind from ~ 20 to ~ 46 au compared to V2 and P10 measurements.

The top right panel of Figure 2 shows the solar wind density as a function of heliocentric distance. The radial profile of the theoretical density and V2 measurements

shows $\sim r^{-2}$, indicating that the densities are inversely proportional to the square of the heliocentric distance. The density observed by P10 is similar to that of V2 until $\sim$ 10 au, then it is relatively larger than that measured by V2 from $\sim$ 10 au to $\sim$ 55 au. Similarly, the solar wind density observed by NH SWAP is higher than that measured by V2 between $\sim$ 22 au and $\sim$ 46 au. This clearly shows that the solar wind density measured by V2, P10, and NH SWAP is different, which may lead to the different radial profiles of entropy shown in Figure 1.

The bottom left panel of Figure 2 plots the theoretical and observed thermal pressure as a function of heliocentric distance, and shows that the theoretical and observed thermal pressure is approximately similar with increasing heliocentric distance. The bottom right panel shows the solar wind proton temperature as a function of heliocentric distance. In the figure, the theoretical temperature and the temperature observed by V2 show similar radial profiles, where both results increase beyond $\sim$ 20 au. However, the temperature measured by P10 is similar to that measured by V2 until $\sim$ 32 au, and then decreases slowly with increasing heliocentric distance. The proton temperature measured by V2 in the upwind direction is larger than that measured by P10 in the downwind direction beyond $\sim$ 32 au, indicating that the turbulence in the upwind direction is stronger than that in the downwind direction. To understand the downwind temperature profile requires further study, but does suggest that the distribution of interstellar neutrals in the upwind direction is higher than that in the downwind direction–see Section 2.2 of Zank 1999 [20]. Consequently, the driving of turbulence by pickup ions may be different in the upwind and downwind directions. This requires further investigation. Interestingly, the solar wind proton temperature measured by NH SWAP is relatively low compared to that measured by V2 and P10 between $\sim$ 25 and $\sim$ 36 au, then it is in between V2 and P10 until $\sim$ 42 au, and then is similar to that measured by P10. This result shows that although the proton temperature observed by NH SWAP and V2 is in the upwind direction, there are differences in the measured temperature.

The left panel of Figure 3 compares the theoretical and observed fluctuating magnetic energy as a function of heliocentric distance. The theoretical total fluctuating magnetic energy (solid curve) is in good agreement with that measured by V2 (blue "*"). At 1 au, the quasi-2D fluctuating magnetic energy (dashed curve) is larger than the slab fluctuating magnetic energy (dashed-dotted-dashed curve), and decreases gradually with increasing heliocentric distance. Within $\sim$ 3 au, the slab fluctuating magnetic energy decreases rapidly, and then slowly with increasing distance. The fluctuating magnetic energy corresponding to P10 (red "*") is relatively higher than that measured by V2. This is consistent with the temperature plot shown in Figure 2 (bottom right) that the temperature measured by P10 is higher than that measured by V2, indicating that the dissipation of the high turbulent magnetic energy leads to a high solar wind temperature.

The right panel of figure 3 describes the correlation length of the fluctuating magnetic energy density as a function of heliocentric distance. The correlation length corresponding to the quasi-2D fluctuating magnetic energy (dashed curve) increases monotonically with increasing heliocentric distance. The correlation length corresponding to the slab fluctuating magnetic energy (dashed-dotted-dashed curve) increases slowly until $\sim$ 3 au, and then decreases with increasing heliocentric distance.

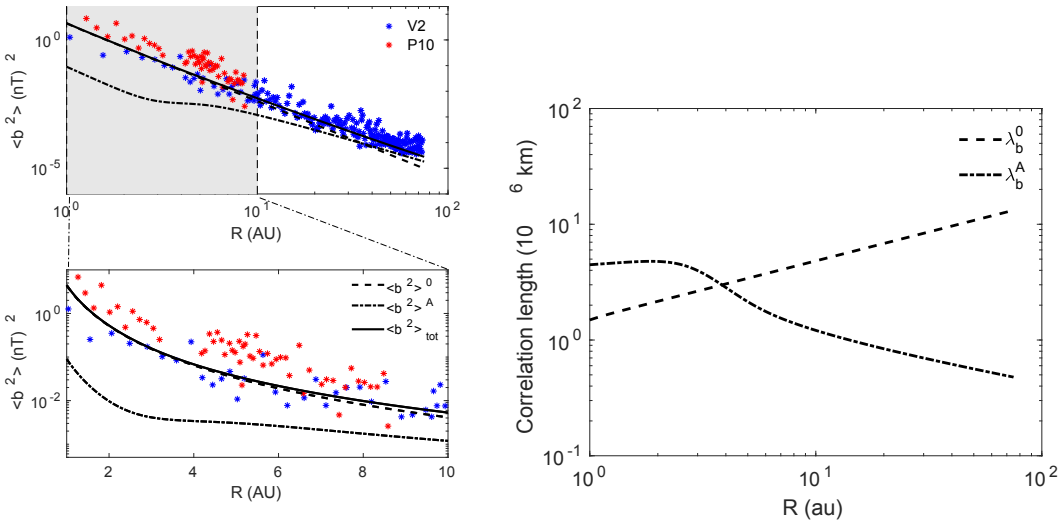

Figure 3. Left panel shows a comparison between the theoretical and observed fluctuating magnetic energy as a function of heliocentric distance. Right panel shows the correlation length as a function of heliocentric distance. The solid curve denotes the total fluctuating magnetic energy, dashed curve the quasi-2D component, and the dashed-dotted the slab component. The blue "*" denotes V2 measurements, and the red "*" P10 measurements.

4. Discussion and Conclusions

We study the evolution of the solar wind entropy using the conservative solar wind and turbulence transport equations developed by Adhikari et al [5], and measurements made by Voyager 2 (V2), Pioneer 10 (P10) and New Horizons Solar Wind Around Pluto (NH SWAP). In this manuscript, we only compare the theoretical results with Voyager 2 measurements. The P10 and NH SWAP measurements provide comparative information about the solar wind parameters throughout the heliosphere. We summarize our findings below.

- The theoretical solar wind entropy and the entropy observed by Voyager 2 show good agreement throughout the heliosphere, and both increase along the trajectory of Voyager 2. Although V2 and NH SWAP follow similar trajectories in the upwind direction, the entropy observed by NH SWAP is relatively lower than that measured by V2, and increases monotonically and slowly with increasing heliocentric distance. Similarly, the entropy measured by P10 in the downwind direction is similar to that of V2 measurement until $\sim$ 36 au, then slowly decreases until $\sim$ 40 au, and then flattens with increasing heliocentric distance.
- V2 and P10 measure solar wind speeds, ranging from $\sim$ 350 kms^{-1} to 550 kms^{-1}, but the speed measured by P10 is lower than that measured by V2 over the distances $\sim 12-18$ au, and $\sim 42-55$ au. The speed measured by NH SWAP does not show a large variation, but is less when compared to V2 and NH SWAP measurements.

- The solar wind density measured by P10 is relatively higher than that measured by NH SWAP and V2. Similarly, the density observed by NH SWAP is comparatively higher than that of V2 measurement.
- The theoretical temperature and the temperature observed by V2 show good agreement with increasing distance, where both increase beyond $\sim$ 20 au. By contrast, P10 observes a monotonic decrease in temperature with increasing distance. The temperature observed by NH SWAP is relatively lower than that measured by V2, and increases slowly beyond $\sim$ 30 au.
- The observed fluctuating magnetic energy corresponding to P10 is relatively larger than that measured by V2. The theoretical fluctuating magnetic energy is similar to that measured by V2.
- The correlation length corresponding to the quasi-2D fluctuating magnetic energy increases gradually with increasing distance. The correlation length corresponding to the NI/slab fluctuating magnetic energy increases slowly until $\sim$ 3 au, and then decreases as distance increases.

Acknowledgments
We acknowledge the partial support of a Parker Solar Probe contract SV4-84017, an NSF-DOE grant PHY-1707247, and an NSF EPSCoR RII-Track-1 cooperative agreement OIA-1655280.

References
[1] Livadiotis G, 2018b *EL* 122 50001
[2] Nicolaou G, Livadiotis G, & Moussas X et al 2014 *SoPh* 289 1371
[3] Livadiotis G, & Desai M I, et al 2016 *ApJ* 829 88
[4] Livadiotis G, 2018a *Entrp* 20 799
[5] Adhikari L, Zank G P, Zhao L -L, and Webb G M et al 2020 *ApJ* 891 34
[6] Whang Y C, Behannon K W, Burlaga L F, & Zhang S et al 1989 *JGR* 94 2345
[7] Whang Y C, Liu S, & Burlaga L F, et al 1990 *JGR* 95 18769
[8] Zank G P, Dosch A, Hunana P, et al 2012 *ApJ* 745 35
[9] Zank G P, Adhikari L, Zhao L -L, et al 2018 *ApJ* 869 23
[10] Richardson J D, & Smith C W, et al 2003 *GeoRL* 30 1206
[11] Elliott H A, McComas D J, Zirnstein E J, et al 2019 *ApJ* 885 156
[12] Zank G P, Matthaeus W H, & Smith C W, et al 1996 *JGR* 101 17093
[13] Zank G P, Adhikari L, Hunana P, et al 2017 *ApJ* 835 147
[14] Adhikari L, Zank G P, Bruno R, et al 2015 *ApJ* 805 63
[15] Adhikari L, Zank G P, Hunana P, et al 2017 *ApJ* 841 85
[16] Isenberg P A, 2005 *ApJ* 623 502
[17] Verdini A, Velli M, Matthaeus W H, Oughton S, & Dmitruk P, et al 2010 *ApJL* 708 L116
[18] Zank G P 2014,*in Transport Processes in Space Physics and Astrophysics* ed G P Zank (*Berlin: Springer*)
[19] Matthaeus W H, Oughton S, Pontius D H Jr, & Zhou Y, et al 1994 *J. Geophys. Res.* 99 19267
[20] Zank G P 1999 *Space Science Reviews* 89 413-688